Published in final edited form as:

Nature. 2010 December 23; 468(7327): 1067–1073. doi:10.1038/nature09504.

Selective inhibition of BET bromodomains

Panagis Filippakopoulos[1,*], **Jun Qi**[2,*], **Sarah Picaud**[1,*], **Yao Shen**[3], **William B. Smith**[2], **Oleg Fedorov**[1], **Elizabeth M. Morse**[2], **Tracey Keates**[1], **Tyler T. Hickman**[4], **Ildiko Felletar**[1], **Martin Philpott**[1], **Shonagh Munro**[5], **Michael R. McKeown**[2,9], **Yuchuan Wang**[6], **Amanda L. Christie**[7], **Nathan West**[2], **Michael J. Cameron**[4], **Brian Schwartz**[4], **Tom D. Heightman**[1], **Nicholas La Thangue**[5], **Christopher A. French**[4], **Olaf Wiest**[3], **Andrew L. Kung**[7,8], **Stefan Knapp**[1,5,**], and **James E. Bradner**[2,9,**]

[1] Department of Clinical Medicine, Structural Genomics Consortium, University of Oxford, Old Road Campus, Roosevelt Drive, Oxford OX3 7DQ, UK

[2] Department of Medical Oncology, Dana-Farber Cancer Institute, Harvard Medical School, 44 Binney Street, Boston, Massachusetts 02115, USA

[3] Walther Cancer Research Center and Department of Chemistry and Biochemistry, University of Notre Dame, Notre Dame, Indiana 46556, USA

[4] Department of Pathology, Brigham & Women's Hospital, Harvard Medical School, 75 Francis Street, Boston, Massachusetts 02115, USA

[5] Department of Clinical Pharmacology, University of Oxford, Old Road Campus, Roosevelt Drive, Oxford OX3 7DQ, UK

[6] Department of Imaging, Dana-Farber Cancer Institute, Harvard Medical School, 44 Binney Street, Boston, Massachusetts 02115, USA

[7] Lurie Family Imaging Center, Dana-Farber Cancer Institute, Harvard Medical School, 44 Binney Street, Boston, Massachusetts 02115, USA

[8] Department of Pediatric Oncology, Dana-Farber Cancer Institute and Children's Hospital, Boston, Harvard Medical School, 44 Binney Street, Boston, Massachusetts 02115, USA

[9] Department of Medicine, Harvard Medical School, 25 Shattuck Street, Boston, MA 02115, USA

**Corresponding authors: James E. Bradner (james_bradner@dfci.harvard.edu), Stefan Knapp (stefan.knapp@sgc.ox.ac.uk).
*These authors contributed equally to this work

Supplementary Information accompanies the paper on www.nature.com/nature.

Author Contributions P.F., J.Q., S.K. and J.E.B. designed the study, analyzed data and wrote the manuscript. P.F. and S.P. performed and analyzed biophysical studies. J.Q. and J.E.B. designed JQ1 and established the synthetic routes. Y.S. and O.W. completed docking and molecular dynamics studies. O.F. performed and analyzed DSF. M.P. and T.H. performed and analyzed alpha-screen assays. W.B.S., M.J.C. and J.E.B. performed *in vitro* NMC studies and IHC. E.M.M performed flow cytometry studies. E.M.M. and N.W. performed proliferation studies. T.T.H., M.J.C., C.A.F. and J.E.B. completed FRAP studies. M.M. and B.S. performed expression analysis. Y.W., A.L.C. and A.L.K. completed *in vivo* efficacy studies. T.K. and I.F. expressed and purified proteins. S.K. and J.E.B. supervised the research.

Author Information Atomic coordinates and structure factors for the reported crystal structures have been deposited with the Protein Data Bank under accession codes 2OSS (BRD4(1)), 3MXF (BRD4(1)/**(+)-JQ1**) and 3ONI (BRD2(2)/**(+)-JQ1**). Reprints and permissions information is available at www.nature.com/reprints. The authors declare no competing financial interests.

Full Methods and any associated references are available online.

Abstract

Epigenetic proteins are intently pursued targets in ligand discovery. To date, successful efforts have been limited to chromatin modifying enzymes, or so-called epigenetic “writers” and “erasers”. Potent inhibitors of histone binding modules have not yet been described. Here we report a cell-permeable small molecule (JQ1) which binds competitively to acetyl-lysine recognition motifs, or bromodomains. High potency and specificity toward a subset of human bromodomains is explained by co-crystal structures with BRD4, revealing excellent shape complementarity with the acetyl-lysine binding cavity. Recurrent translocation of BRD4 is observed in a genetically-defined, incurable subtype of human squamous carcinoma. Competitive binding by JQ1 displaces the BRD4 fusion oncoprotein from chromatin, prompting squamous differentiation and specific anti-proliferative effects in BRD4-dependent cell lines and patient-derived xenograft models. These data establish proof of concept for targeting protein-protein interactions of epigenetic “readers” and provide a versatile chemical scaffold for the development of chemical probes more broadly throughout the bromodomain family.

Gene regulation is fundamentally governed by reversible, non-covalent assembly of macromolecules[1]. Signal transduction to RNA polymerase requires higher-ordered protein complexes, spatially regulated by assembly factors capable of interpreting the post-translational modification states of chromatin[2]. Readers of epigenetic marks are structurally diverse proteins each possessing one or more evolutionarily conserved effector modules, which recognize covalent modifications of histone proteins or DNA. The ε-N-acetylation of lysine residues (Kac) on histone tails is associated with an open chromatin architecture and transcriptional activation[3]. Context-specific molecular recognition of acetyl-lysine is principally mediated by bromodomains.

Bromodomain-containing proteins are of substantial biological interest, as components of transcription factor complexes and determinants of epigenetic memory[4]. There are 41 diverse human proteins containing a total of 57 bromodomains. Despite large sequence variations, all bromodomain modules share a conserved fold comprising a left-handed bundle of four alpha helices (α_Z, α_A, α_B, α_C), linked by diverse loop regions (ZA and BC loops) that contribute to substrate specificity. Co-crystal structures with peptidic substrates showed that the acetyl-lysine is recognized by a central hydrophobic cavity and is anchored by a hydrogen bond with an asparagine residue present in most bromodomains[5]. The bromodomain and extra-terminal (BET) family (BRD2, BRD3, BRD4 and BRDT) shares a common domain architecture comprising two N-terminal bromodomains which exhibit high levels of sequence conservation, and a more divergent C-terminal recruitment domain (Supplementary Fig. 1)[6].

Recent research has established a compelling rationale for targeting BRD4 in cancer. BRD4 remains bound to transcriptional start sites of genes expressed during the M/G1 transition, influencing mitotic progression[4]. BRD4 is also a critical mediator of transcriptional elongation, functioning to recruit the positive transcription elongation factor complex (P-TEFb)[7],[8]. Cyclin dependent kinase-9, a core component of P-TEFb[9]–[11], is a validated target in chronic lymphocytic leukemia[12], and has recently been linked to c-Myc dependent

transcription[13]. Thus, BRD4 recruits P-TEFb to mitotic chromosomes resulting in increased expression of growth promoting genes[14].

Importantly, BRD4 has recently been identified as a component of a recurrent t(15;19) chromosomal translocation in an aggressive form of human squamous carcinoma[15,16]. Such translocations express the tandem N-terminal bromodomains of BRD4 as an in-frame chimera with the NUT (nuclear protein in testis) protein, genetically defining the so-called NUT midline carcinoma (NMC). Functional studies in patient-derived NMC cell lines have validated the essential role of the BRD4-NUT oncoprotein in maintaining the characteristic proliferation advantage and differentiation block of this uniformly fatal malignancy[17]. Notably, RNA silencing of BRD4-NUT arrests proliferation and prompts terminal squamous differentiation. These observations underscore the broad utility and immediate therapeutic potential of a direct-acting inhibitor of human bromodomain proteins.

A selective and potent inhibitor for the BET sub-family of bromodomains

A major collaborative focus of our research groups concerns the development of chemical probes[18,19] and the optimization of therapeutic leads for the translation of small-molecule modulators of epigenetic targets as cancer therapeutics. Motivated by the above rationale, we have developed biochemical platforms for the identification of new inhibitors of bromodomain isoforms using high-throughput screening, as well as the annotation of putative ligands emerging from collaborative and published research. In the course of these studies, we learned of a remarkable observation by Mitsubishi Pharmaceuticals that simple thienodiazepines possessed binding activity for BRD4[20]. Prior research from this group suggests these compounds emerged from anti-inflammatory phenotypic studies, such as inhibition of CD28 co-stimulation as a means of treating autoimmune diseases[21,22]. A rich literature has established the synthetic accessibility and favorable pharmacologic properties of this privileged class of drug-like small molecules[23]. Indeed, the core scaffold described appears in FDA-approved substances such as alprazolam and triazolam.

Inferring structure-activity-relationships also derived from molecular modeling of candidate ligands within the binding pocket of the apo crystal structure of the first bromodomain of BRD4 (hereafter referred to as BRD4(1); PDB ID 2OSS), we designed a prototype ligand, **JQ1** (Fig. 1a). **JQ1** is a novel thieno-triazolo-1,4-diazepine, possessing an appended, bulky *t*-butyl ester functional group at C6 in order to (1) allow for additional pendant group diversity, as needed, and (2) to mitigate binding to the central benzodiazepine receptor as predicted by published SAR[23]. We first established a high-yielding, seven step synthetic route to access racemic **JQ1** (hereafter referred to as **JQ1**) and derivatives (Scheme S1, Supplemental Methods). We have also identified a route to synthesize each enantiomer, **(+)-JQ1** and **(−)-JQ1** (Scheme S2, Supplemental Methods).

To establish a biochemical platform for comprehensive selectivity screening, all human bromodomains were subcloned into bacterial expression vectors. Testing of an average of 15 expression constructs per bromodomain target resulted in the identification of 37 expression systems that yielded soluble protein suitable for specificity screening and covered all bromodomain subfamilies (Supplementary Table 1). Since the specific substrates of most

bromodomains are unknown, a general binding assay based on differential scanning fluorimetry (DSF) was implemented[24]. Binding of **(+)-JQ1** significantly increased the thermal stability of all bromodomains of the BET family (Fig. 1b, Supplementary Table 2) with ΔT_mobs values between 4.2 °C (BRDT(1)) and 10.1 °C (BRD4(1)). No significant stability shifts were detected for bromodomains outside the BET family, suggesting that this ligand is highly selective. In contrast, the stereoisomer **(−)-JQ1** showed no significant interaction with any bromodomain present in our panel.

Within a family of proteins a linear correlation between DSF ΔT_mobs values and binding constants has been observed, with temperature shifts larger than 6 °C corresponding to compounds with nM dissociation constants[25],[26]. Since the sensitivity of this assay may vary between different protein families, isothermal titration calorimetry (ITC) was used to precisely determine binding constants. Enantiomerically pure **(+)-JQ1** bound with a K_d of about 50 nM and 90 nM to the first and second bromodomains of BRD4, respectively (Fig. 1c, Supplementary Table 3). Comparable binding to both domains of BRD3 was observed, whereas the first bromodomains of BRDT and BRD2 revealed about 3-fold weaker binding. Affinities determined by ITC and ΔT_mobs values showed very good correlation (Fig. 1d). Importantly, **(+)-JQ1** showed no detectable binding to bromodomains that exhibited minimal temperature shifts, such as WDR9(2) and CREBBP.

To assess whether **(+)-JQ1** binding was competitive with acetyl-lysine, we adapted a luminescence proximity homogeneous assay (ALPHA-screen)[27] to the BET bromodomains. Binding of a tetra-acetylated Histone H4 peptide to BRD4 was strongly inhibited by **(+)-JQ1**, with IC_{50} values of 77 nM and 33 nM for the first and second bromodomain, respectively (Fig. 1e). The IC_{50} for the **(−)-JQ1** stereoisomer against BRD4(1) and for **(+)-JQ1** against CREBBP were both estimated to be above 10,000 nM (Fig. 1e). Thus, **(+)-JQ1** represents a potent, highly specific and Kac competitive inhibitor for the BET family of bromodomains.

(+)-JQ1 binds to the acetyl-lysine binding site of BET-family bromodomains

In order to establish the binding mode of **JQ1** we determined co-crystal structures using racemic material and purified, recombinant BRD4(1) and BRD2(2) (for data collection and refinement statistics see Supplementary Table 4). The determined high resolution structures revealed only the **(+)-JQ1** enantiomer bound directly into the Kac binding site (Fig. 2, Fig. 3a, b). Similar to interactions observed in acetyl-lysine complexes[28], the triazole ring formed a hydrogen bond with the evolutionarily conserved asparagine (Asn140 in BRD4(1) and Asn429 in BRD2(2); Fig. 2a). The inhibitor showed an extraordinary shape complementarity with the Kac binding site, occupying the entire binding pocket (Fig. 2c, d). In both complexes, ligand binding was stabilized by hydrophobic interactions with conserved BET residues in the ZA- and BC-loop regions (Fig. 3a, b). Structural and sequence comparison showed high conservation of the BET Kac binding pocket, but revealed a number of differences in loop regions lining the binding cavity that could be explored for future development of isoform specific inhibitors (Fig. 3a, b, c).

Docking of either isomer of **JQ1** to BRD4(1) resulted in excellent fit of **(+)-JQ1** in a position of perfect overlap to the crystallographically determined binding mode, while **(−)-JQ1** resulted in an energetically unfavourable conformation with significant distortion of the diazepine ring system due to steric clashes with residues of the ZA-loop region (Fig. 3d). To explore the dynamic features of BET bromodomains, we carried out 20 ns molecular dynamics simulations (MD) of BRD4(1) in the absence and presence of **(+)-JQ1**. The simulations revealed little displacement of the protein helixes, but the loop regions surrounding the acetyl-lysine binding site exhibited significant conformational flexibility. Furthermore, these loops were much more flexible in the absence (Fig. 3e) than in the presence (Fig. 3f) of the inhibitor, suggesting that **(+)-JQ1** stabilized the Kac binding cavity. In all cases, MD simulation energies converged (Supplementary Fig. 2).

JQ1 displaces BRD4 from nuclear chromatin in cells

To establish whether **JQ1** binds bromodomains competitively with chromatin in a cellular environment, we performed fluorescence recovery after photobleaching (FRAP) experiments. Prior research has demonstrated the utility of FRAP in assessing the pace of lateral redistribution of human bromodomains[17,29]. Human osteosarcoma cells (U2OS) transfected with a GFP-BRD4 exhibit a time-dependent recovery of fluorescence intensity (Fig. 4a, b). In the presence of **JQ1** (500 nM), observed recovery is immediate, suggesting displaced and freely diffusing nuclear BRD4 (Fig. 4a, b). Cellular FRAP studies confirmed that effects on the mobile fraction of BRD4 are limited to the biochemically active **(+)-JQ1** stereoisomer (Supplemental Fig. 3).

Having demonstrated potent, selective binding to BRD4 in homogeneous and cell-based assays, we became interested to explore effects of **JQ1** on disease-relevant phenotypes. Prior studies have established that the pathogenic BRD4-NUT fusion protein arising from t(15;19) translocation in NMC binds avidly to discrete foci of acetylated chromatin, conferring a proliferative advantage and differentiation block[17]. Using FRAP, we assessed the ability of **JQ1** to target directly the BRD4-NUT oncoprotein. Compared to a vehicle control, **JQ1** (500 nM) markedly accelerated time to half fluorescence recovery in photobleached regions of cells transfected with GFP-BRD4-NUT (Fig. 4c, d). Importantly, no effect was observed on redistribution of GFP-NUT (Supplementary Fig. 3). These data are consistent with competitive binding of **JQ1** to BRD4 in cultured cells.

JQ1 induces squamous differentiation and growth arrest in BRD4-dependent carcinoma

Direct inhibition of gene products expressed from recurrent, oncogenic translocations is a validated therapeutic approach in cancer[30,31]. We thus endeavoured to establish the consequences of competitive inhibition of BRD4-NUT in NMC. A characteristic feature of NMC is the appearance of discrete nuclear speckles of the BRD4-NUT oncoprotein by NUT-directed immunohistochemistry (IHC)[32]. Treatment of the patient-derived 797 NMC cell line for 48 hours with **JQ1** (500 nM) effaces nuclear foci, producing diffuse nuclear NUT staining by IHC (Supplementary Fig. 3e). In a dose- and time-dependent manner, **JQ1** provokes a differentiation phenotype in NMC cell lines, featuring cell spreading and

flattening, open chromatin and striking spindle morphology (Fig. 4e; Supplementary Fig. 4). Differentiation is prompt (< 24 hours) and characterized by dramatic changes in cell shape accompanied by markedly augmented expression of cytokeratin, a hallmark of squamous differentiation (Fig. 4e). After seven days in culture with sub-micromolar exposures to **JQ1**, terminal differentiation is observed. In this manner, **JQ1** phenocopies the morphologic changes and increased keratin expression observed with BRD4-NUT silencing by RNA interference (Supplementary Fig. 5)[17]. Corroborating these studies, expression analysis of three canonical squamous tissue genes by RT-PCR identified marked (30-fold) induction of Keratin-14 by **(+)-JQ1** in NMC 797 cells (Fig. 4f). The modest induction of keratin-10 without affecting epidermal transglutaminase (TGM1) may indicate differentiation toward thoracic squamous epithelium, consistent with the mediastinal primary tumor from which NMC 797 cells derive[33]. Induction of differentiation with strong (3+) keratin staining is progressive over 72 h, as determined by quantitative IHC analysis (Supplementary Fig. 6). Supporting an on-target mechanism-of-action, the **(−)-JQ1** enantiomer is comparatively inactive in NMC, and a non-BRD4-dependent squamous carcinoma cell line (TE10) fails to exhibit differentiation effects of active **JQ1** (Supplementary Fig. 4c).

In BRD4-dependent NMC cells, differentiation is expectedly accompanied by growth arrest, evidenced by reduced Ki67 staining (Supplementary Fig. 7), sustained inhibition of proliferation (Fig. 4g; Supplementary Fig. 8) and G1 cell cycle arrest (Fig. 4h). To further understand the observed G1 arrest and to confirm an effect of **JQ1** on known BRD4-dependent genes, we performed quantitative RT-PCR for Rad21 and Ran[4]. **(+)-JQ1** potently decreased expression of both BRD4 target genes, whereas **(−)-JQ1** had no effect (Fig. 4f). Early and late apoptosis were assessed with annexin-V and propidium iodide staining to ascertain whether the antiproliferative effect and irreversible differentiation was accompanied by cell death. Indeed, **JQ1** induces immediate and progressive apoptosis in BRD4-dependent human carcinoma cells, without triggering significant growth arrest or cell death in cell lines lacking the BRD-NUT fusion (Supplementary Fig. 8, 9).

Pharmacodynamic and anti-tumor efficacy of JQ1 in xenograft models of NMC

To determine whether **JQ1** could attenuate the growth of BRD4-dependent carcinoma as a single agent *in vivo*, we developed three mouse xenograft models of NMC in mice. First, short-term treatment studies were performed in NMC 797 xenografts with positron-emission tomography (PET) imaging of ^{18}F-fluorodeoxyglucose (FDG) uptake as a primary endpoint to explore whether activity of **JQ1** could be demonstrated by non-invasive imaging. Matched cohorts of mice with established tumors were randomized to treatment with **JQ1** (50 mg kg^{-1}) or vehicle, administered by daily intraperitoneal injection. Prior to randomization, and after four days of therapy, mice were evaluated by FDG-PET imaging. A marked reduction in FDG uptake was observed with **JQ1** treatment, whereas vehicle-treated animals demonstrated progressive disease (Fig. 5a). Tumor-volume measurements confirmed a reduction in tumor growth with **JQ1** treatment (Fig. 5b and Supplementary Fig. 10). **JQ1** was well tolerated at this dose and schedule without overt signs of toxicity or weight loss (Supplementary Fig. 10b).

To confirm that the anti-neoplastic effect observed with **JQ1** treatment was associated with target engagement, sectioned tumor tissue was examined for the BRD4-NUT oncoprotein. As presented in Supplementary Figure 11, **JQ1** treatment resulted in effacement of NUT nuclear speckles, consistent with competitive binding to nuclear chromatin. Cell spreading and increased keratin expression confirmed induction of squamous differentiation (Fig. 5c). Decreased nuclear Ki67 and increased TUNEL staining in treated animals confirmed an ongoing anti-proliferative, pro-apoptotic effect (Supplementary Fig. 11). To quantify the pharmacodynamic biomarker of tumor keratin expression, we established protocols for automated IHC image acquisition and analysis. Paired samples from treated and untreated animals were prepared and analyzed using standardized protocols and commercially-available software (ImageScope; Aperio Technologies), demonstrating that **JQ1** induced strong (3+) keratin expression in NMC 797 xenografts, (Supplementary Fig. 12).

In parallel with these studies, we had occasion to care for a 29 year-old patient with widely metastatic BRD4-NUT positive NMC arising from the mediastinum. With the goal of developing a more clinically-relevant disease model, we established short-term cultures (11060 cells) using discarded clinical material obtained from pleural fluid draining from a palliative chest tube. As presented in Supplementary Figure 13, *in vitro* studies confirmed the stereospecific, potent effect of **(+)-JQ1** on cellular viability (IC50 = 4 nM), growth and cell cycle progression. Four animals engrafted with patient-derived tumor material developed measurable disease, which was strongly FDG-avid by PET imaging (Fig. 5d). Animals were randomly assigned to vehicle or **(+)-JQ1** treatment. Prior to treatment and after four days of therapy, mice were evaluated by PET imaging. A marked response in FDG uptake was observed with **(+)-JQ1** treatment, whereas vehicle-treated animals demonstrated progressive disease (Fig. 5e). Tumor material prepared for quantitative IHC analysis demonstrated induction of keratin expression following **(+)-JQ1** treatment (Fig. 5f–g, Supplementary Fig. 14) in this minimally-passaged NMC xenograft model.

To confirm the translational potential of direct-acting BRD4 inhibition in NMC, we further adapted the patient-derived 11060 cells to expansion *in vivo*, and performed definitive efficacy studies. Marked tumor regression and improved overall survival were observed, following only 18 days of well-tolerated therapy with **(+)-JQ1** (Fig. 5h–i). These results were recapitulated in a third NMC xenograft model, using Per403 cells (Fig 5j–k, Supplementary Fig. 15). Together, these data establish *in vivo* proof-of-concept for targeting BRD4 with **JQ1** in NMC.

Discussion

Across the complex landscape of the cancer genome, recurrent chromosomal rearrangements comprise a compelling subset of clear, genetic targets in cancer. As evidenced by the successful development of first- and second-generation kinase inhibitors targeting BCR-ABL in CML, well-characterized probe compounds[34,35], high-resolution crystallographic data[36], translational research studies[37], and informative murine models[38], where available, provide an optimal platform for ligand discovery and target validation. Herein, we provide evidence supporting the BRD4-NUT fusion as a therapeutic target in an incurable,

genetically-defined human squamous carcinoma, using a novel BRD4-directed small molecule inhibitor.

Beyond NUT-midline carcinoma, BET-family bromodomains contribute to other neoplastic and non-neoplastic diseases. BRD4 targets the P-TEFb complex to mitotic chromosomes resulting in expression of growth promoting genes such as c-Myc[12,14] and the well established cancer target Aurora B[39]. BET family members have been recognized as essential genes for the replication of viruses[40,41] and in mediating inflammatory responses[42]. Thus, the availability of **(+)-JQ1** will prompt informative research broadly in developmental and disease biology. **JQ1** possesses many desirable qualities of a chemical probe, such as high target potency in homogeneous and cellular assays, a well-characterized profile of selectivity, synthetic accessibility and herein proven utility in experimental biology[18,19]. We have also found **JQ1** to exhibit few off-target effects on cellular receptors and excellent pharmacokinetic properties including 49% oral bioavailability (Supplementary Fig. 16, 17 and Supplementary Table 5), establishing the plausibility of developing drug-like derivatives for therapeutic application.

The discovery and optimization of small-molecule inhibitors of epigenetic targets is a major focus of current biomedical research. We sought to meet the challenge of developing potent, selective inhibitors of epigenetic readers. Here, we present a first, thoroughly characterized inhibitor of the BET-family of bromodomains. The approach outlined herein further establishes the feasibility of abrogating protein-protein interactions with small molecules, and targeting additional epigenetic readers for ligand discovery.

Methods Summary

The inhibitor **JQ1** was synthesized in both racemic and enantiomerically pure format using the synthetic route outlined in Scheme S1 and Scheme S2 and its structure was fully characterized. Human bromodomains were expressed in bacteria as His-tagged proteins and were purified by nickel-affinity and gel-filtration chromatography. Proteins integrity was assessed by SDS-PAGE and Electro-spray Mass Spectrometry on an Agilent 1100 Series LC/MSD TOF. All crystallizations were carried out at 4 °C using the sitting drop vapour-diffusion method. X-ray diffraction data were collected at the Swiss Light source beamline X10SA, or using a Rigaku FR-E generator. Structures were determined by molecular replacement. Isothermal titration calorimetry experiments were performed at 15 °C on a VP-ITC titration microcalorimeter (MicroCal™). Thermal melting experiments were carried out on a Mx3005p RT- PCR machine (Stratagene) using SYPRO Orange as a fluorescence probe. Dose-ranging small-molecule studies of proliferation were performed in white, 384-well plates (Corning) in DMEM media containing 10 % FBS. Compounds were delivered with a PerkinElmer JANUS pin-transfer robot and Envision multilabel plate-reader, using a commercial assay (Cell TiterGlo). Murine xenografts were established by injecting NMC cells in 30 % Matrigel (BD Biosciences) into the flank of 6 week-old female NCr nude mice (Charles River Laboratories). Tumor measurements were assessed by caliper measurements, and volume calculated using the formula $Vol = 0.5 \times L \times W^2$. All mice were humanely euthanized, and tumors were fixed in 10 % formalin for histopathological examination. Quantitative immunohistochemistry was performed using the Aperio Digital Pathology

Environment (Aperio Technologies, Vista, CA) at the DF/HCC Core Laboratory at the Brigham and Women's Hospital.

Supplementary Material

Refer to Web version on PubMed Central for supplementary material.

Acknowledgments

We are grateful to Drs. Udo Oppermann, Susanne Müller, Stephen Sallan, Christopher Lathan, Peter Rahl, Richard Young, Kevin Lee and Katharin Shaw for thoughtful discussions and sharing unpublished information; Kachicholu Agu, Stephen Johnston and Li Li for analytical chemistry support; John Daley for flow cytometry support; Teri Bowman, Tyler Caron, Corey Marvin and Dr. Scott Rodig for IHC; and Adam Bass for sharing cell lines. The Structural Genomics Consortium is a registered charity (number 1097737) that receives funds from the Canadian Institutes for Health Research, the Canadian Foundation for Innovation, Genome Canada through the Ontario Genomics Institute, GlaxoSmithKline, Karolinska Institutet, the Knut and Alice Wallenberg Foundation, the Ontario Innovation Trust, the Ontario Ministry for Research and Innovation, Merck & Co., Inc., the Novartis Research Foundation, the Swedish Agency for Innovation Systems, the Swedish Foundation for Strategic Research and the Wellcome Trust. This research was supported by a Graduate Fellowship from the Chemistry-Biochemistry-Biology Interface Program at the University of Notre Dame, NIGMS T32-075762 (to Y.S.), the DF/HCC (to C.A.F. and J.E.B.), the National Institutes of Health, the Burroughs Wellcome Fund, and the Leukemia & Lymphoma Society (to J.E.B.).

References

1. Ptashne M. Binding reactions: epigenetic switches, signal transduction and cancer. Curr Biol. 2009; 19:R234–241. [PubMed: 19321137]
2. Schreiber SL, Bernstein BE. Signaling network model of chromatin. Cell. 2002; 111:771–778. [PubMed: 12526804]
3. Marushige K. Activation of chromatin by acetylation of histone side chains. Proc Natl Acad Sci U S A. 1976; 73:3937–3941. [PubMed: 1069278]
4. Dey A, Nishiyama A, Karpova T, McNally J, Ozato K. Brd4 marks select genes on mitotic chromatin and directs postmitotic transcription. Mol Biol Cell. 2009; 20:4899–4909. [PubMed: 19812244]
5. Owen DJ, et al. The structural basis for the recognition of acetylated histone H4 by the bromodomain of histone acetyltransferase gcn5p. Embo J. 2000; 19:6141–6149. [PubMed: 11080160]
6. Zeng L, Zhou MM. Bromodomain: an acetyl-lysine binding domain. FEBS Lett. 2002; 513:124–128. [PubMed: 11911891]
7. Yang XJ. Multisite protein modification and intramolecular signaling. Oncogene. 2005; 24:1653–1662. [PubMed: 15744326]
8. Yang Z, et al. Recruitment of P-TEFb for stimulation of transcriptional elongation by the bromodomain protein Brd4. Mol Cell. 2005; 19:535–545. [PubMed: 16109377]
9. Peng J, Zhu Y, Milton JT, Price DH. Identification of multiple cyclin subunits of human P-TEFb. Genes Dev. 1998; 12:755–762. [PubMed: 9499409]
10. Marshall NF, Price DH. Purification of P-TEFb, a transcription factor required for the transition into productive elongation. J Biol Chem. 1995; 270:12335–12338. [PubMed: 7759473]
11. Marshall NF, Peng J, Xie Z, Price DH. Control of RNA polymerase II elongation potential by a novel carboxyl-terminal domain kinase. J Biol Chem. 1996; 271:27176–27183. [PubMed: 8900211]
12. Phelps MA, et al. Clinical response and pharmacokinetics from a phase 1 study of an active dosing schedule of flavopiridol in relapsed chronic lymphocytic leukemia. Blood. 2009; 113:2637–2645. [PubMed: 18981292]
13. Rahl PB, et al. c-Myc Regulates Transcriptional Pause Release. Cell. 2010; 141:4323–4445.

14. Yang Z, He N, Zhou Q. Brd4 recruits P-TEFb to chromosomes at late mitosis to promote G1 gene expression and cell cycle progression. Mol Cell Biol. 2008; 28:967–976. [PubMed: 18039861]
15. French CA, Miyoshi I, Aster JC, et al. BRD4 bromodomain gene rearrangement in aggressive carcinoma with translocation t (15;19). Am J Pathol. 2001; 159(6):1987–1992. [PubMed: 11733348]
16. French CA, et al. BRD4-NUT fusion oncogene: a novel mechanism in aggressive carcinoma. Cancer Res. 2003; 63:304–307. [PubMed: 12543779]
17. French CA, et al. BRD-NUT oncoproteins: a family of closely related nuclear proteins that block epithelial differentiation and maintain the growth of carcinoma cells. Oncogene. 2008; 27:2237–2242. [PubMed: 17934517]
18. Frye SV. The art of the chemical probe. Nat Chem Biol. 6:159–161. [PubMed: 20154659]
19. Oprea TI, et al. A crowdsourcing evaluation of the NIH chemical probes. Nat Chem Biol. 2009; 5:441–447. [PubMed: 19536101]
20. Miyoshi, S.; Ooike, S.; Iwata, K.; Hikawa, H.; Sugaraha, K. ANTITUMOR AGENT. MITSUBISHI TANABE PHARMA CORPORATION; 2009. p. 1-37.
21. Adachi, K., et al. MITSUBISHI TANABE PHARMA CORPORATION; 2006. p. 1-240.
22. Sueoka, H.; Komatsu, H.; Kobayashi, H.; Ehara, S. Thienotriazolodiazepine compounds and medicinal uses thereof. YOSHITOMI PHARMACEUTICAL INDUSTRIES, LTD; 1998. p. 1-50.
23. VonVoigtlander PF, Straw RN. Alprazolam: Review of Pharmacological, Pharmacokinetic and Clinical Data. Drug Development Research. 1985; 6:1–12.
24. Niesen FH, Berglund H, Vedadi M. The use of differential scanning fluorimetry to detect ligand interactions that promote protein stability. Nat Protoc. 2007; 2:2212–2221. [PubMed: 17853878]
25. Fedorov O, et al. A systematic interaction map of validated kinase inhibitors with Ser/Thr kinases. Proc Natl Acad Sci U S A. 2007; 104:20523–20528. [PubMed: 18077363]
26. Bullock AN, et al. Structural basis of inhibitor specificity of the human protooncogene proviral insertion site in moloney murine leukemia virus (PIM-1) kinase. J Med Chem. 2005; 48:7604–7614. [PubMed: 16302800]
27. Quinn AM, et al. A homogeneous method for investigation of methylation-dependent protein-protein interactions in epigenetics. Nucleic Acids Res. 2010; 38:e11. [PubMed: 19897549]
28. Vollmuth F, Blankenfeldt W, Geyer M. Structures of the dual bromodomains of the P-TEFb-activating protein Brd4 at atomic resolution. J Biol Chem. 2009; 284:36547–36556. [PubMed: 19828451]
29. Dey A, et al. A bromodomain protein, MCAP, associates with mitotic chromosomes and affects G(2)-to-M transition. Mol Cell Biol. 2000; 20:6537–6549. [PubMed: 10938129]
30. Huang ME, et al. Use of all-trans retinoic acid in the treatment of acute promyelocytic leukemia. Blood. 1988; 72:567–572. [PubMed: 3165295]
31. Druker BJ, et al. Efficacy and safety of a specific inhibitor of the BCR-ABL tyrosine kinase in chronic myeloid leukemia. N Engl J Med. 2001; 344:1031–1037. [PubMed: 11287972]
32. Haack H, et al. Diagnosis of NUT midline carcinoma using a NUT-specific monoclonal antibody. Am J Surg Pathol. 2009; 33:984–991. [PubMed: 19363441]
33. Toretsky JA, et al. Translocation (11;15;19): a highly specific chromosome rearrangement associated with poorly differentiated thymic carcinoma in young patients. Am J Clin Oncol. 2003; 26:300–306. [PubMed: 12796605]
34. Buchdunger E, et al. Selective inhibition of the platelet-derived growth factor signal transduction pathway by a protein-tyrosine kinase inhibitor of the 2-phenylaminopyrimidine class. Proc Natl Acad Sci U S A. 1995; 92:2558–2562. [PubMed: 7708684]
35. Buchdunger E, et al. Inhibition of the Abl protein-tyrosine kinase in vitro and in vivo by a 2-phenylaminopyrimidine derivative. Cancer Res. 1996; 56:100–104. [PubMed: 8548747]
36. Schindler T, et al. Structural mechanism for STI-571 inhibition of abelson tyrosine kinase. Science. 2000; 289:1938–1942. [PubMed: 10988075]
37. Druker BJ, et al. Effects of a selective inhibitor of the Abl tyrosine kinase on the growth of Bcr-Abl positive cells. Nat Med. 1996; 2:561–566. [PubMed: 8616716]

38. le Coutre P, et al. In vivo eradication of human BCR/ABL-positive leukemia cells with an ABL kinase inhibitor. J Natl Cancer Inst. 1999; 91:163–168. [PubMed: 9923858]

39. You J, et al. Regulation of aurora B expression by the bromodomain protein Brd4. Mol Cell Biol. 2009; 29:5094–5103. [PubMed: 19596781]

40. You J, et al. Kaposi's sarcoma-associated herpesvirus latency-associated nuclear antigen interacts with bromodomain protein Brd4 on host mitotic chromosomes. J Virol. 2006; 80:8909–8919. [PubMed: 16940503]

41. Abbate EA, Voitenleitner C, Botchan MR. Structure of the papillomavirus DNA-tethering complex E2:Brd4 and a peptide that ablates HPV chromosomal association. Mol Cell. 2006; 24:877–889. [PubMed: 17189190]

42. Huang B, Yang XD, Zhou MM, Ozato K, Chen LF. Brd4 coactivates transcriptional activation of NF-kappaB via specific binding to acetylated RelA. Mol Cell Biol. 2009; 29:1375–1387. [PubMed: 19103749]

43. Cole PA. Chemical probes for histone-modifying enzymes. Nat Chem Biol. 2008; 4:590–597. [PubMed: 18800048]

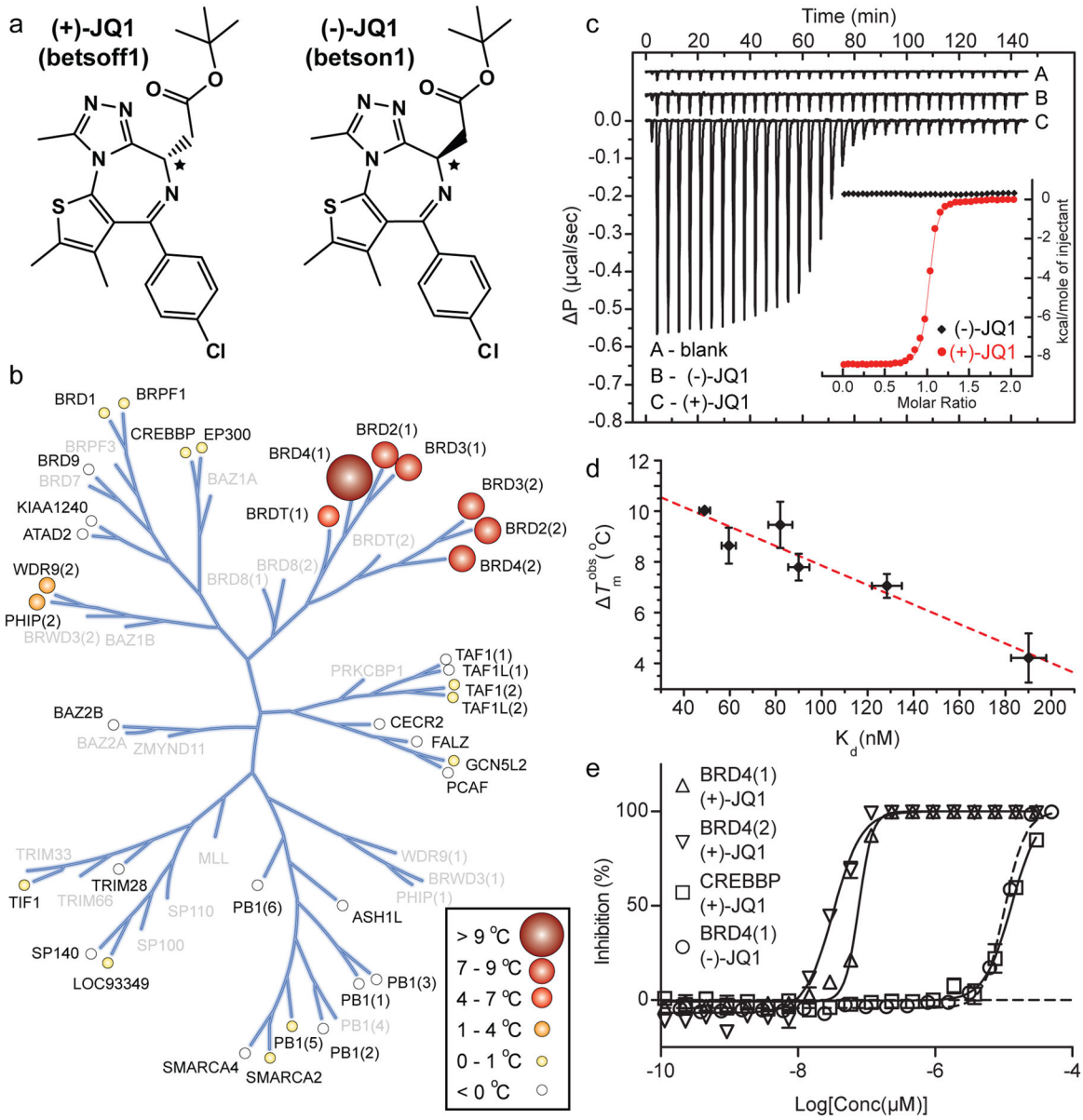

Figure 1. Structure and selectivity of JQ1

a, Structure of the two **JQ1** stereo-isomers. The stereocentre at C6 is indicated by an asterix (*). **b,** Assessment of inhibitor selectivity using Differential Scanning Fluorimetry (DSF). Shown are averaged temperature shifts (ΔT_m^{obs}) in °C upon binding of 10 μM **(+)-JQ1**. The temperature shifts are represented by spheres as indicated in the inset. Screened proteins are labelled and proteins not included in the selectivity panel are shown in grey. **(−)-JQ1** did not reveal any significant temperature shifts to any of the screened bromodomains. **c,** Isothermal Titration Calorimetry (ITC). Raw injection heats are shown for a blank titration of (BRD4(1)) into buffer (A), and reverse titrations using the inactive isomer **(−)-JQ1** (B) and the active isomer **(+)-JQ1** (C). The inset shows normalized binding enthalpies corrected for the heat of dilution as a function of binding site saturation (symbols as indicated in the inset). Solid lines represent a nonlinear least squares fit using a single-site binding model. **d,**

Thermal shifts (ΔT_m^{obs}) show good correlation to dissociation constants (K_d) determined by ITC for the BET bromodomains. The dotted red line represents a least squares fit with an R of 96 %. **e,** Competitive displacement of a histone peptide from human bromodomains is exhibited by **JQ1** using a bead-based proximity assay. Alpha screen titrations monitoring the displacement of a tetra-acetylated histone H4 peptide by **JQ1** isomers using the bromodomains BRD4(1), BRD4(2) or of an acetylated H3 peptide using CREBBP.

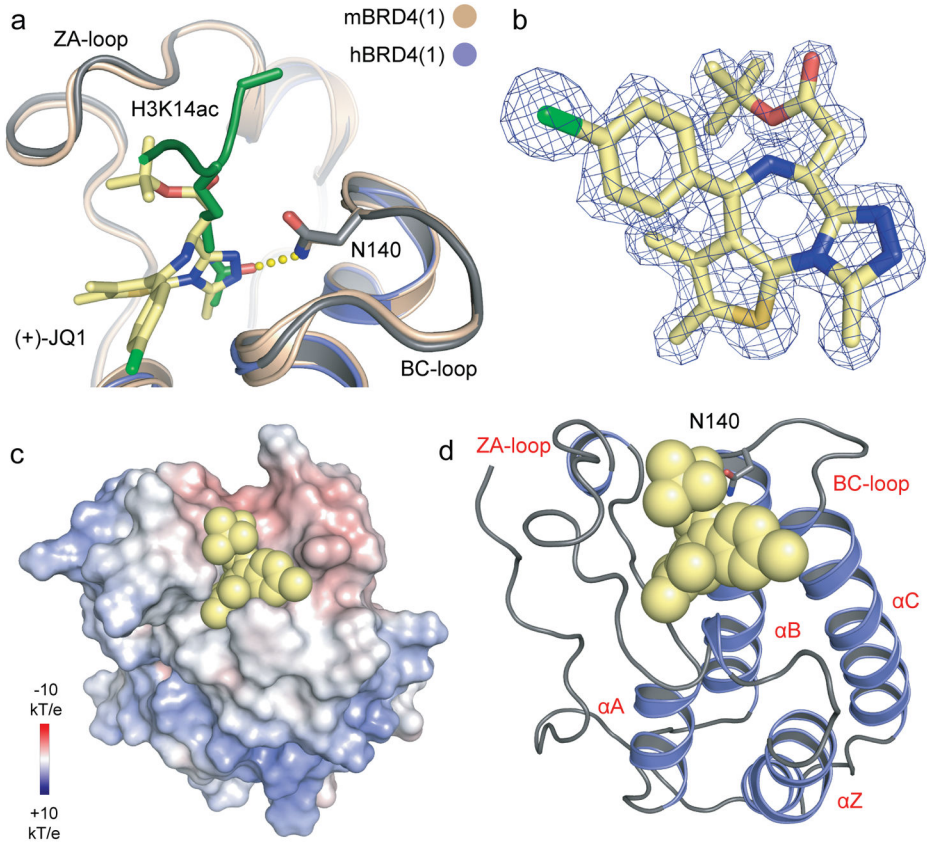

Figure 2. Characterization of BET complexes with (+)-JQ1

a, Superimposition of the mouse BRD4(1)/H3K14ac peptide complex[28] with the human BRD4(1)/**(+)-JQ1** complex structure. The hydrogen bond formed to the conserved asparagine (N140) in the peptide complex is shown as yellow dots. **b,** $2F_o$-F_c map of **(+)-JQ1** in complex with BRD4(1) contoured at 2σ. **c,** Electrostatic surface of BRD4(1) in complex with **(+)-JQ1**. The ligand is shown as a CPK model demonstrating the excellent shape complimentarity with the protein acetylated lysine receptor site. **d,** Ribbon diagram of the complex of human BRD4(1) with **(+)-JQ1** in CPK representation. The main secondary structural elements and the conserved active site asparagine side chain (N140) are labelled.

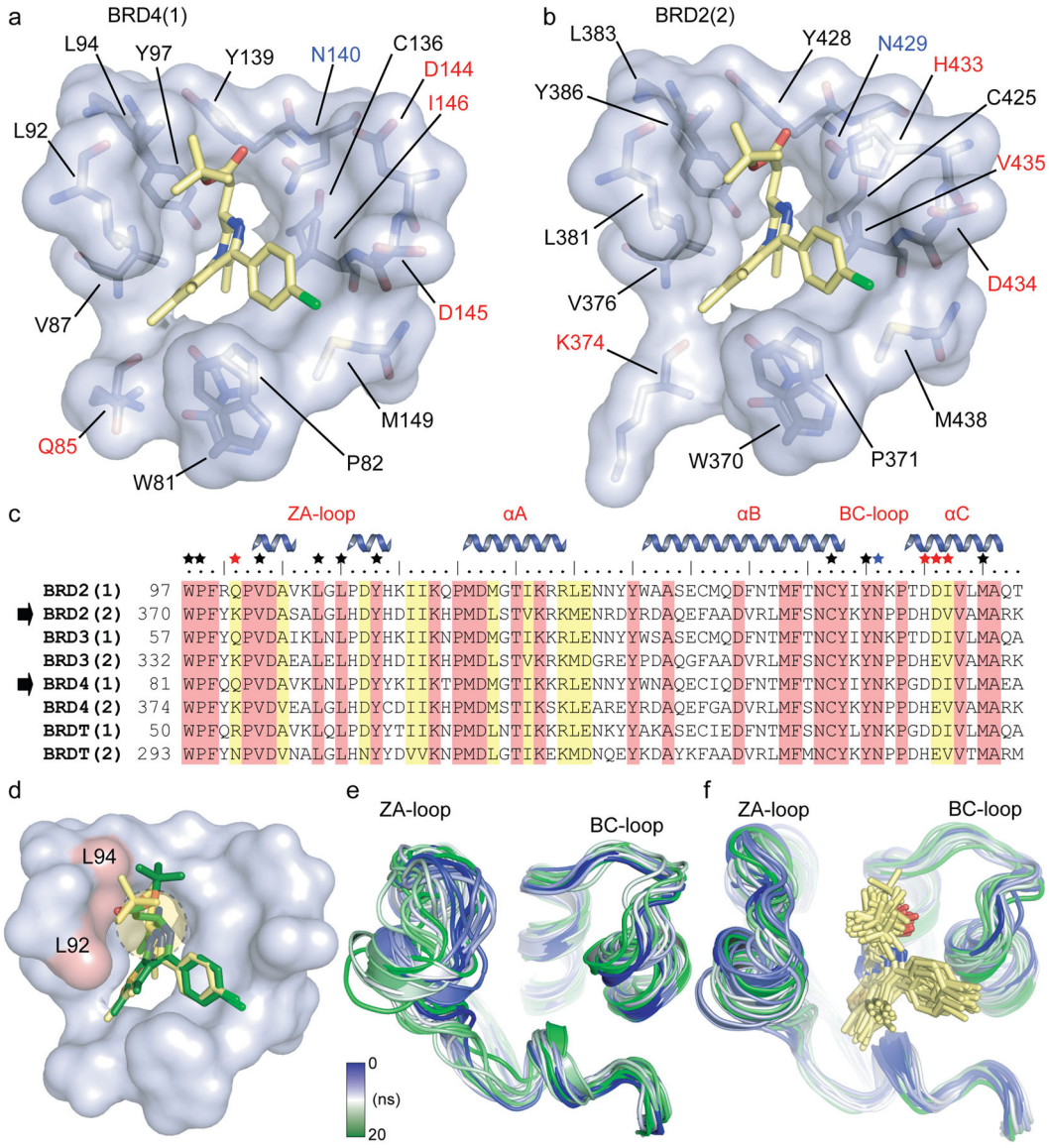

Figure 3. Binding site comparison between N- and C- terminal bromodomains in complex with (+)-JQ1

a, The acetyl-lysine binding pocket of BRD4(1) is shown as a semitransparent surface with contact residues labelled and depicted in stick representation. Carbon atoms in **(+)-JQ1** are coloured yellow to distinguish them from protein residues. **b,** The acetyl-lysine binding pocket of BRD2(2) is shown in identical representation and orientation as described in (**a**). **c,** Protein sequence alignment of the human BET subfamily highlighting conserved (red) and similar (yellow) residues. Major bromodomain structural elements are shown. The side-chain contacts with **(+)-JQ1** are annotated with a black star. Contacts which differ between the N- and C-terminal BET bromodomains (red star) are highlighted. The family conserved asparagine is indicated by a blue star. **d,** Models of **(+)-JQ1** (in yellow) and **(−)-JQ1** (in green) docked into the BRD4(1) binding site. The steric clashes of the **(−)-JQ1** stereo-isomer with Leu92 and Leu94 are highlighted in red. **e,** MD simulation demonstrating the

flexibility of the ZA- and BC- loops of the BRD4(1) apo-structure. Shown are the backbone of BRD4(1) during a 20 ns simulation as snapshots separated by 1 ns intervals. The different structures are distinguished by colours changing from blue to green as indicated in the inset. **f,** MD simulation of the BRD4(1)/**(+)-JQ1** complex depicted in 1 ns snapshots as described in (**e**).

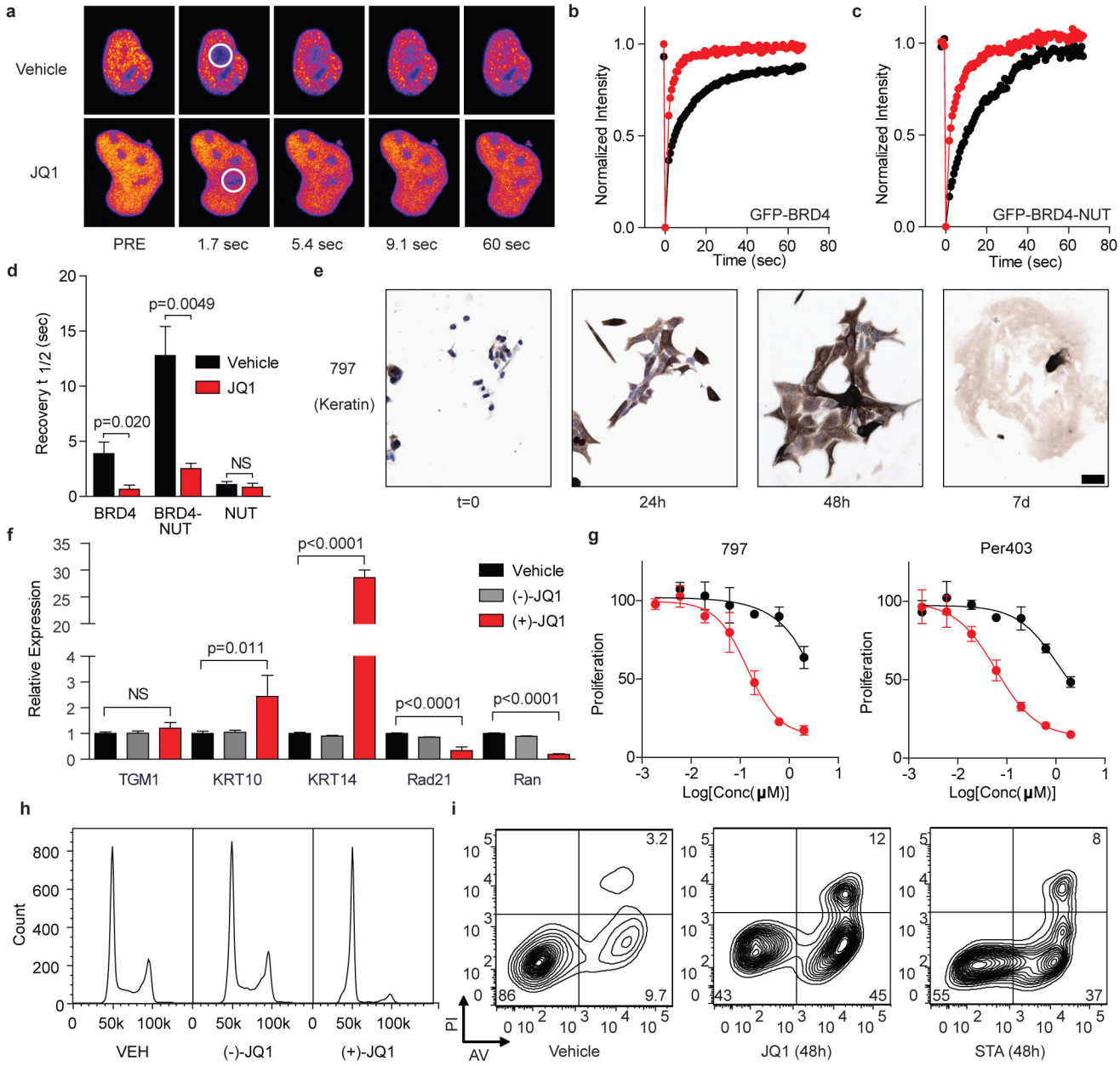

Figure 4. JQ1 binds BRD4 competitively with chromatin resulting in differentiation and growth arrest of NMC cells

a, Fluorescence recovery after photobleaching (FRAP) of GFP-BRD4 demonstrates enhanced recovery in the presence of **JQ1**. Nuclei are false-colored in proportion to fluorescence intensity. White circles indicate target regions of photobleaching. **b–c**, **JQ1** accelerates fluorescence recovery in FRAP experiments performed with transfected (**b**) GFP-BRD4 and (**c**) GFP-BRD4-NUT. **d**, Quantitative comparison of time to half-maximal fluorescence recovery for FRAP studies (**b–c,** Supplementary Fig. 3a). Data represent the mean ± s.d. (n = 5), and are annotated with *p*-values as obtained from a two-tailed *t*-test. **e**, Differentiation of NMC cells by **JQ1** (500 nM) is prompt and characterized by a marked increase in cytokeratin expression (AE1/AE3; 10x, scale bar is 50 μm). **f**, Comparative gene

expression studies of **(+)-JQ1** (red; 250 nM, 48 h) versus **(−)-JQ1** (gray; 250 nM, 48 h) and vehicle (black) confirm squamous differentiation. Data represent the mean ± s.d. (n = 3), and are annotated with *p*-values as obtained from a two-tailed *t*-test. **g,** Growth effects of BRD4 inhibition on BRD4-NUT dependent cell lines. Cells were incubated with **(+)-JQ1** (red circles) or **(−)-JQ1** (black circles) and monitored for proliferation after 72 hours. **(+)-JQ1** uniquely attenuates proliferation by NMC cell lines. Data is presented as mean ± s.d. (n = 3). Curve fit was calculated by logistic regression. **h**, Flow cytometry for DNA content in NMC 797 cells. **(+)-JQ1** (250 nM, 48 h) induces a G1 arrest compared to **(−)-JQ1** (250 nM) and vehicle control. **i**, Flow cytometric analysis of NMC 797 squamous carcinoma cells treated with vehicle, **JQ1** or staurosporine (STA), as indicated. PI, propidium iodide. AV, annexin-V.

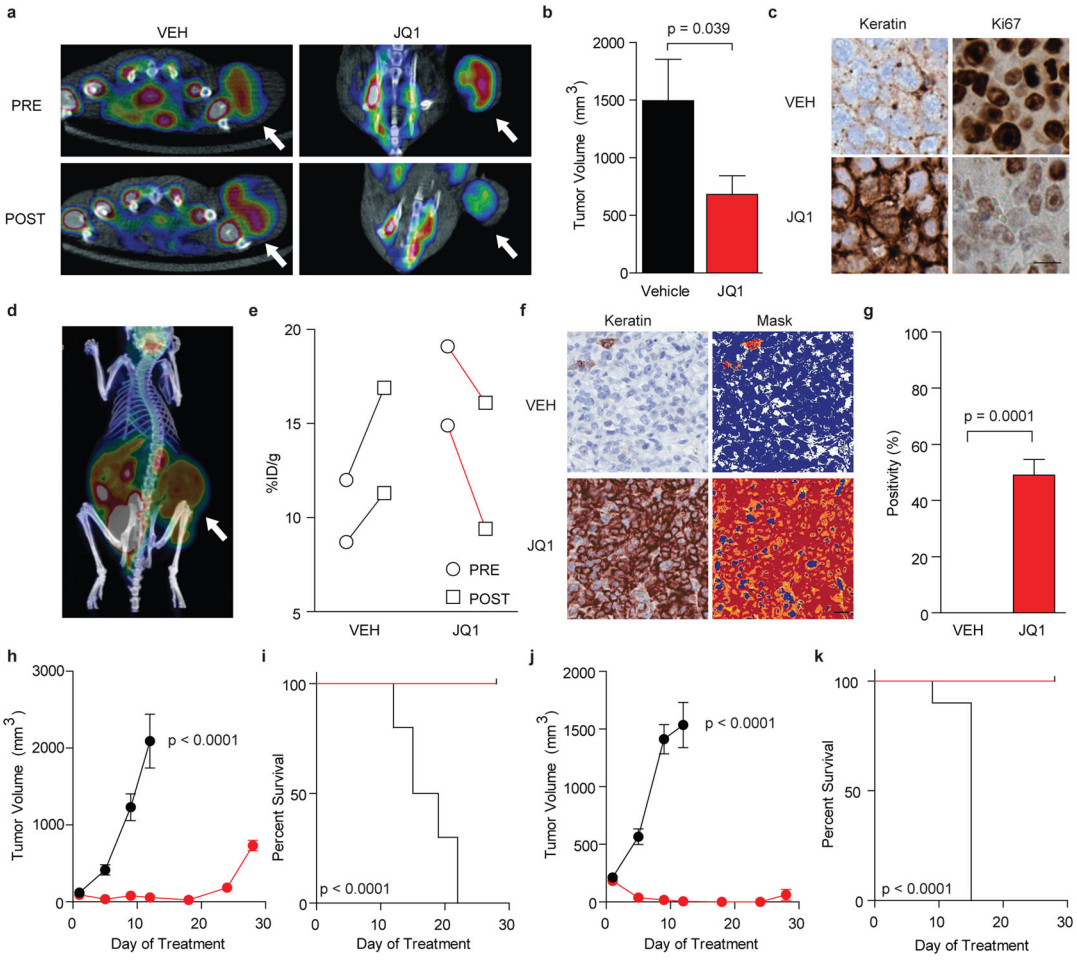

Figure 5. JQ1 promotes differentiation, tumor regression and improved survival in murine models of NMC

a, PET imaging of murine NMC 797 xenografts. FDG uptake in xenograft tumors is reduced by 50 mg kg $^{-1}$ **JQ1** treatment compared to vehicle control. **b**, Tumor volume is reduced in mice with established disease (NMC 797 xenografts) treated with 50 mg kg $^{-1}$ daily **JQ1** compared to vehicle control. A significant response to therapy is observed by two-tailed *t*-test at 14 days ($p = 0.039$). Data represent the mean ± s.d. (n = 7). **c**, Histopathological analysis of NMC 797 tumors excised from animals treated with **JQ1** reveals induction of keratin expression (AE1/AE3, 40x) and impaired proliferation (Ki67, 40x), as compared to vehicle-treated animals (scale bar is 20 μm). **d**, Viability of patient-derived NMC 11060 xenografts was confirmed by PET imaging. **e**, Therapeutic response of primary 11060 NMC xenografts to **(+)-JQ1** (50 mg kg $^{-1}$ daily for four days) was demonstrated by PET imaging. **f**, Histopathological analysis of primary NMC 11060 tumors excised from animals treated with **(+)-JQ1** reveals induction of keratin expression (AE1/AE3, 20x; scale bar is 20 μm), compared to vehicle-treated animals. Quantitative analysis of keratin induction was performed using image masking (**f**, right panel) and pixel positivity analysis (**g**). A significant response to therapy is observed by two-tailed *t*-test ($p = 0.0001$). Data represent the mean ± s.d. of three independent wide microscopic fields. Comparative images of stained excised tumors and quantitative masks are provided in Supplementary Figure 14. **h–**

k, **(+)-JQ1** (50 mg kg $^{-1}$ daily for 18 days) produces a decrease in tumor volume (**h, j**) and promotes improved survival (**i, k**) in patient-derived 11060 (**h, i**) and Per403 (**j, k**) NMC xenograft models (n=10 in all groups). A significant response to therapy is observed for tumor volume by two-tailed *t*-test ($p < 0.0001$) and for overall survival by a log-rank test ($p < 0.0001$).